CrossMark

RESEARCH PAPER

Seasonal effects on geophysical–geotechnical relationships and their implications for electrical resistivity tomography monitoring of slopes

R. M. Hen-Jones[1,5] · P. N. Hughes[2] · R. A. Stirling[1] · S. Glendinning[1] · J. E. Chambers[3] · D. A. Gunn[3] · Y. J. Cui[4]

Abstract Current assessments of slope stability rely on point sensors, the results of which are often difficult to interpret, have relatively high costs and do not provide large-area coverage. A new system is under development, based on integrated geophysical–geotechnical sensors to monitor groundwater conditions via electrical resistivity tomography. So that this system can provide end users with reliable information, it is essential that the relationships between resistivity, shear strength, suction and water content are fully resolved, particularly where soils undergo significant cycles of drying and wetting, with associated soil fabric changes. This paper presents a study to establish these relationships for a remoulded clay taken from a test site in Northumberland, UK. A rigorous testing programme has been undertaken, integrating the results of multi-scalar laboratory and field experiments, comparing two-point and four-point resistivity testing methods. Shear strength and water content were investigated using standard methods, whilst a soil water retention curve was derived using a WP4 dewpoint potentiometer. To simulate seasonal effects, drying and wetting cycles were imposed on prepared soil specimens. Results indicated an inverse power relationship between resistivity and water content with limited hysteresis between drying and wetting cycles. Soil resistivity at lower water contents was, however, observed to increase with ongoing seasonal cycling. Linear hysteretic relationships were established between undrained shear strength and water content, principally affected by two mechanisms: soil fabric deterioration and soil suction loss between drying and wetting events. These trends were supported by images obtained from scanning electron microscopy.

Keywords Electrical resistivity tomography · Soil water retention · Soil cracking · Undrained shear strength

1 Introduction

Approximately one-third of the total asset value of the UK transport network is derived from infrastructure slopes [43]. Maintaining this network is costly; it is estimated that in the UK, Network Rail spent £70 million in 2007/2008 on preventative works to stabilize earthworks [17, 44]. Projections of future climate change suggest a move towards drier summers and wetter winters [15], with associated changes in ground condition and hence implications for slope stability. It is well understood that increasing groundwater decreases soil strength and can lead to swelling of some clay soils [18] and that conversely drying increases soil strength but causes shrinkage and desiccation cracking [50]. These moisture-driven changes have the potential to increase the incidence of failure across a range of earth structures [27, 30], affecting road and rail networks. Whilst the magnitude of these impacts is not fully understood, engineers and asset managers require reliable and cost-effective systems to monitor the condition of these assets and direct maintenance activities at the most vulnerable parts of the network.

✉ R. M. Hen-Jones
  rose.hen-jones@bristol.ac.uk

1 School of Civil Engineering and Geosciences, Newcastle University, Newcastle-upon-Tyne NE1 7RU, UK

2 School of Engineering and Computer Sciences, Durham University, Durham DH1 3LE, UK

3 British Geological Survey, Nottingham NG12 5GG, UK

4 Laboratoire Navier/CERMES, Ecole des Ponts ParisTech, Cité Descartes, 77455 Champs-Sur-Marne, France

5 Department of Civil Engineering, University of Bristol, Bristol BS8 1TW, UK

Traditionally, groundwater monitoring in engineering applications has been performed through the use of piezometers and tensiometers [12, 19, 52] which have increased in sophistication and reduced in price over time. However, direct monitoring in this way remains expensive (from both an equipment and human resource perspective) and is only able to provide single point values which may be unreliable and require much effort to resolve a spatially integrated cross-sectional model. Monitoring of ground movement over larger areas can be accomplished using aerial reconnaissance and LIDAR and is done regularly by asset owners such as Network Rail [4], but these surveys provide topographical information only [31] and therefore are not currently capable of capturing potentially rapid changes in subsurface conditions preceding slope failure.

Risk-based early interventions are required to prevent failure of these assets, with unplanned repairs costing up to ten times more than preventative actions [26]. However, such interventions require monitoring systems capable of identifying changes in the internal conditions that precede failure, in real time. Geoelectrical imaging methods such as electrical resistivity tomography (ERT) have the potential to provide a cost-effective monitoring solution to this problem [9, 25].

Electrical resistivity tomography is a ground imaging technique that is being increasingly applied to the characterisation and monitoring of the subsurface [35]. Resistivity is particularly sensitive to changes in pore fluid resistivity and saturation as the principal mode of current flow in the subsurface is through electrolytic conduction in the pore fluid [47]; consequently, ERT is widely used in hydrogeophysical investigations [3, 56]. ERT can also be used to distinguish between lithologies of contrasting resistivity, where resistivity can vary due to differing porosities [2] or due to the presence of clay minerals [46, 48]. Clay minerals exert a particularly strong influence on resistivity due to electric conduction on the clay mineral surface—hence an increasing proportion of clay in a soil or rock is generally linked to a reduction in resistivity [54]. Although there are an increasing number of studies using three-dimensional ERT (using electrode arrays) as a means of characterising and monitoring unstable slopes [10, 23, 38, 42], relevant geophysical–geotechnical relationships require further validation. As elevated water contents and a corresponding reduction in soil suction are associated with shear failure, their interaction with soil resistivity is key to the development of a slope stability assessment system.

Many studies have investigated the relationship between electrical resistivity and water content for clays both in the laboratory [24, 33, 37] and in the field [11, 39]. However, in order to fully resolve these relationships, it is necessary to investigate how they are affected by repeated seasonal cycles, which have been shown to progressively weaken clay fills [36]. This process is likely to be exacerbated by the increasingly frequent and extreme weather events suggested by climate change projections. Studies on partially saturated rocks [45] and sands [32, 34] observed hysteresis in the electrical response to varying degrees of saturation between imbibition (wetting) and drainage; a study by Muñoz-Castelblanco et al. [40] on a natural unsaturated loess found soil resistivity to be independent of whether a drying or a wetting path was followed. However, there is little research into the effects of repeated seasonal cycles on the resistivity response of volume-sensitive clay soils. Hysteresis in near-surface soils is well established in the soil water retention curve [20, 22, 49] whereby at a given water content a decrease in soil suction is observed between the drying and the wetting paths, due to entrapped air. Associated decreases in soil strength may then be a function of both this suction loss and soil fabric changes incurred by desiccation cracking.

Given the hysteretic nature of these geotechnical relationships, it is necessary to understand how soil strength, suction and resistivity interact when subjected to seasonally varying water content, in order to be able to interpret geophysical information gathered from electrical resistivity tomography arrays. This study aims to investigate geophysical–geotechnical property inter-relationships in engineered clay fills and particularly the evolution of these relationships resulting from soil fabric changes associated with seasonal moisture cycling. To this end, a comprehensive experimental programme integrating field monitoring and multi-scale laboratory tests has been undertaken on clay material obtained from the full-scale test embankment in Northumberland, UK, which forms part of the BIONICS field research project [27, 30]. A suite of laboratory tests simulating seasonal field conditions has been performed, targeted at resolving the effects of dry-wet cycles on geotechnical and geophysical properties, complementing ongoing field monitoring at BIONICS, which is used as a basis for comparison. The effects of seasonally varying environmental conditions were also evaluated at the micro-scale in order to investigate resultant soil fabric deterioration. In this research paper, all three approaches are integrated in order to understand the effects of extreme weather events on the inter-relationships, which are essential to the success of a slope stability monitoring system based on electrical resistivity tomography.

2 Test site and material properties

The BIONICS embankment was constructed in 2005, from a locally sourced glacial till (Durham Lower Boulder Clay). It was compacted to a dry density of approximately 1.6 Mg/m^3 and has an average in situ water content of

22%, with a corresponding bulk density of 2.01 Mg/m^3. The embankment is 90 m long, 6 m high, 29 m wide and with a 5 m crest and 1 in 2 slopes, orientated along its length in an East to West direction. This geometry was chosen so as to be representative of typical UK infrastructure embankments based on the report published by Perry et al. [43].

The Atterberg limits of the clay, tested in accordance with BS 1377-2: 1990 [5], were 45 and 24% for Liquid and Plastic Limits, respectively (average values calculated from 12 No. tests), which classifies the fill material to be of intermediate plasticity, with a USCS classification CL [1]. The results of quantitative XRD analyses on the sub-2-μm fraction of the embankment fill material suggest that the clay mineral assemblages are generally similar and composed of variable amounts of illite/smectite (ranging from 42 to 54%, with a mean of 49%), chlorite/smectite (3–7% range, mean 5%), illite (16–26% range, mean 19%) and kaolinite (23–31% range, mean 26%). In all cases, the separated sub-2-μm fractions also contain small quantities of quartz and lepidocrocite (γ-FeOOH).

Laboratory assessment of compaction characteristics of the clay soil was performed according to BS 1377-4: 1990 [7]. Using normal Proctor compaction, the maximum dry density of the embankment fill was measured to be 1.71 Mg/m^3 at an optimum water content (w_{opt}) of 15.5%, and the modified compaction maximum dry density was measured to be 1.80 Mg/m^3 at a w_{opt} of 13% [27].

3 Method

In order to achieve the stated aim, a series of laboratory and field experiments have been conducted on clay soil recovered from the BIONICS site. Geotechnical–geophysical property changes resulting from seasonal cycling were investigated by laboratory testing; data gathered during field monitoring served as a basis for comparison. Trends observed in both the laboratory and the field were then investigated at the micro-scale using microscopy techniques to image resultant changes in soil structure. Densities and water contents measured in situ at the test site were replicated as starting conditions for the laboratory tests, in order to allow for direct comparison with field results. Undrained shear strength (C_u) was investigated, such that water content remained constant throughout the test: the authors acknowledge that this test does not allow for measurement of pore pressures during testing. It is recognised, however, as representative of short-term behaviour [55] which is relevant to slope stability assessments, particularly when considering rapid changes in subsurface conditions, such as those associated with extreme rainfall. Although partially saturated specimens

were tested (thus not constituting a "true" value of undrained shear strength), the term C_u has been used to describe the measurement, given that it does describe the maximum shear resistance encountered during undrained shearing. Undrained triaxial testing of partially saturated soils is described in Fredlund and Rahardjo [21].

Considering the above, three main phases of testing were undertaken:

I. Resistivity–geotechnical property relationships (laboratory and field).
II. Soil water retention behaviour (laboratory).
III. Imaging of soil fabric changes (microscopy).

For all the laboratory tests, specimens were subjected to cycles of either drying or imbibition (wetting). The specific methodologies used to achieve this are described in Sects. 3.1, 3.2, 3.3; a summary of these methodologies and the saturation history of the datasets included in this paper are provided in Table 1.

Phases I, II and III relate to laboratory testing of different sample batches. Air-drying was achieved in a 20 °C temperature-controlled environment. Following preparation and moisture cycling, all specimens were wrapped in plastic film and left to homogenise for 24 h.

Bulk clay soil was passed through a 20-mm sieve and allowed to air-dry for 24 h. The dried soil was then crushed using a mechanical crusher with a 3-mm plate separation, and passed through a 2-mm sieve. Deionised water was added to the processed soil in order to bring it to a water content of 22%. After a homogenisation period of 24 h, this soil was compacted into test specimens, the dimensions of which varied according to the test to be conducted. Specific details of the specimen preparation procedure for each type of test are discussed below.

3.1 Phase I. Resistivity–geotechnical relationships

Seventy-five 38 mm diameter by 76 mm length cylindrical soil specimens were prepared using a steel mould filled by tamping after the addition of each of four approximately equal layers, creating a deliberately rough interface between the layers. 173.5 g of soil was weighed out per specimen, corresponding to target densities described in Sect. 2. Following preparation, specimens were moisture cycled, as follows: drying was achieved by allowing specimens to air-dry until their masses corresponded to target water contents, at regular intervals between 22% and the residual; wetting was achieved by allowing specimens to reach their residual water content, and then wetted up by placing specimens in a "humidity chamber" [an insulated box with two 90 ml/h mist generators submerged in

Table 1 Drying and wetting cycles imposed upon BIONICS clay laboratory datasets

Stage	Dataset	Method of moisture cycling
1		
(a) Drying	Phase I (SWRC)	Air-drying
	Phase II (water content–resistivity–shear strength)	Air-drying
	Phase III (soil fabric imaging)	Evacuation during imaging
(b) Wetting	Phase I (SWRC)	Hand-powered water mister
	Phase II (water content–resistivity–shear strength)	Humidifying chamber
	Phase III (soil fabric imaging)	Addition of droplet
2		
(a) Re-drying	Phase II (water content–resistivity–shear strength)	Air-drying
(b) Re-wetting	Phase II (water content–resistivity–shear strength)	Humidifying chamber

deionised water, with a grate above to hold the specimens (Fig. 1)].

Twenty-five specimens were used to create Stage 1a (drying), eighteen for Stage 1b (wetting), sixteen for Stage 2a (re-drying) and sixteen for Stage 2b (re-wetting). Specimens were tested for resistivity using the two-point method, in accordance with BS 1377-3 [6]. To improve contact resistance at the soil–electrode interface, the disc electrodes were coated with a layer of Nyogel 756 conductive grease, of conductivity 3.33 S/m [41]. Specimens were then subjected to the quick undrained triaxial test under a confining pressure of 100 kPa and a strain rate of 1.27 mm/min, in accordance with BS 1377-7 [8] Following failure, the middle third of each clay specimen was oven-dried to determine exact water content.

In addition to the above tests, it was decided to investigate the effects of desiccation cracking on soil resistivity, using the two-point method. In order to stimulate desiccation cracks, fourteen specimens were prepared

with inbuilt planes of weakness which would be more vulnerable to cracking as shrinkage occurred during drying. This was achieved by tamping after the addition of each of the four layers, creating a deliberately smooth surface, orthogonal to the direction of current flow. For this series of tests, only Stage 1a (drying) was performed.

For all of the two-point resistivity tests described above, a resistivity measurement error of $\pm14\%$ was calculated, assuming an error of 0.5 mm for measurement of specimen dimensions, equating to an error of 3.5% for the geometric factor K (A/L). Errors pertaining to voltage and current measurement were calculated to be 0.5% and 10%, respectively, based on the resolution of the instrumentation. These errors pertain solely to the repeatability of the data and do not account for contact resistances between the specimen and the electrodes, which are incorporated within the two-point resistivity measurement. Large contact resistances can cause soil resistivity to be overestimated [28, 29] and, therefore, a
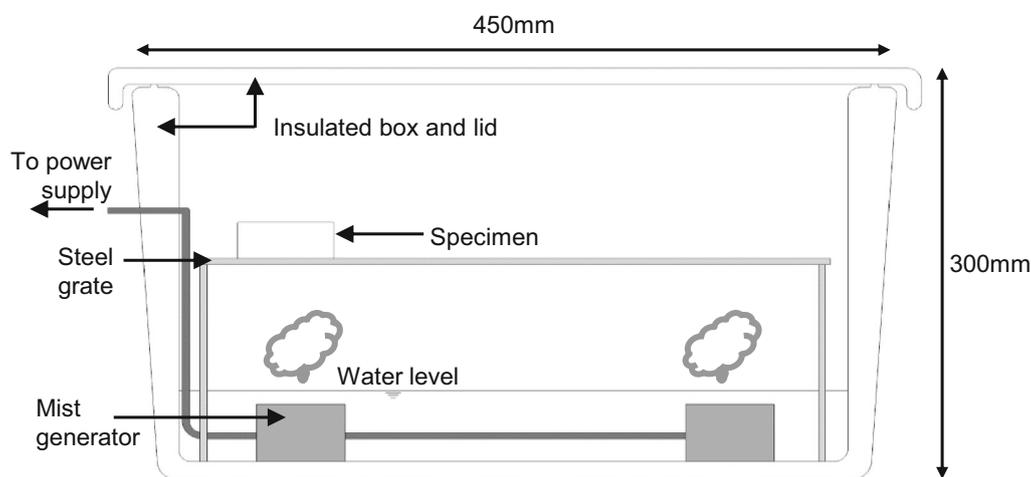
Fig. 1 Humidity chamber

comparison of two- and four-point resistivity methods was also performed in this study.

Clay was compacted into three bespoke resistivity test chambers by tamping after the addition of each of four layers. The test chambers comprised a rectangular prism with square plate electrodes at both ends, for injecting current, with point electrodes inserted through the casing into the compacted clay specimen, for measurement of potential difference (Fig. 2, below). The inner dimensions of the resistivity test chambers were 78 mm × 25 mm × 25 mm, with a plate electrode separation of 75 mm, pin electrode separation of 25 mm, introduced to a depth of 5 mm into the specimens. A four-point drying curve (Stage 1a) was produced, following the Wenner method described in BS 1377-3: 1990; the outer electrodes were then used to obtain a two-point measurement for the same specimen. For all resistivity measurements, a resistivity error was calculated, assuming a 0.5-mm error in measurement of specimen dimensions, equating to an error of 4% in the geometric factor. Errors pertaining to the instrumentation summed to 8%, yielding a total error of ±12%.

In order to generate field data for comparison against laboratory-derived resistivity water content relationships, in situ resistivity and water content measurements were taken using a Decagon 5TE soil moisture, temperature and electrical conductivity sensor. These were installed at two depths (0.5 and 1.0 m) in a south-facing slope of the BIONICS testing embankment (described in Sect. 2) between 02/06/2013 and 26/07/2013, when the embankment was experiencing a drying period. Volumetric water content is measured using a frequency domain system to an accuracy of ±15%; electrical conductivity is measured using a two-point resistivity-measuring system to an accuracy of ±10% [14].

3.2 Phase II. Soil water retention curve (SWRC)

Thirteen 38 mm diameter × 8 mm length discs were formed by placing 18.5 g of moistened clay (at 22% water content) into a compaction cell at a strain rate of 0.33 mm/min until the target length was achieved. The specimens were subjected to moisture cycling in the following ways: drying was achieved by allowing the specimens to air-dry until their masses corresponded to target water contents at regular intervals between 22% and the residual; wetting was achieved by spraying specimens using a hand-powered water mister. The reason for the difference in wetting procedure with respect to Phase I specimens is the smaller volume of these specimens such that they required a less intense wetting environment to achieve a given moisture content. Eight specimens were used for Stage 1a (drying), whilst five specimens were reserved for Stage 1b (wetting). Specimens were put in a WP4 dewpoint potentiometer [13], and their pore pressures recorded before being oven-dried to confirm their water content. Further detail on the test procedure can be found in Stirling and Hen-Jones [51].

The Van Genuchten [53] expression was fitted to the water content–suction data to create a soil water retention curve (SWRC) for the initial drying and wetting stages of the clay.

3.3 Phase III. Imaging of soil fabric changes

The results from Phase I, investigation of resistivity–geotechnical relationships, showed a progressive loss in shear strength with an associated increase in resistivity between primary and secondary drying paths (Figs. 6 and 7). It was suggested that this could be attributed to deterioration of the soil fabric itself, resulting from extreme moisture cycling. In order to investigate the presence of microstructural changes upon extreme drying, imaging with fields of view down to 10 μm was carried out using an environmental scanning electron microscope (E-SEM). This technique enabled the temperature and pressure of the immediate atmosphere around the specimen to be prescribed in order to control humidity and ultimately, drying rate. Specimens of the sieved BIONICS material were prepared to the liquid limit and homogenised before being compacted into 10-mm-circular steel specimen holders to a depth of 5 mm. Small
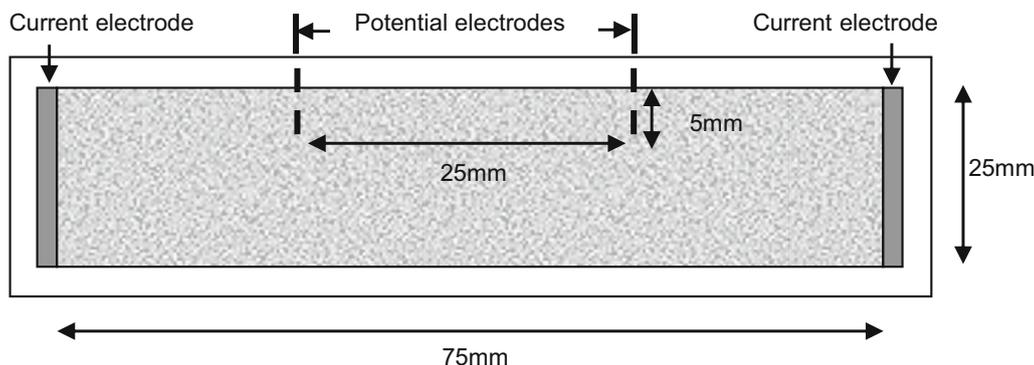

Fig. 2 Plan view of open-topped resistivity chamber with plate current and point potential electrodes

steel holders were selected on the basis of being a low mass, thermally conductive medium between the cooling stage of the instrument and the specimen. Specimen holders comprised an internally ribbed texture to aid interface adhesion and inhibit the material from shrinking freely. A drying environment was promoted by a reduction in relative humidity within the imaging chamber following initial reference imaging. Specimens were then rewet by the addition of a droplet of water and allowed to homogenise for 24 h before retesting. The reason for the difference in moisture cycling procedure for phase III specimens is the considerably smaller volume of soil, on which tests showed the other wetting procedures to be ineffective.

4 Results

All of the data presented below are shown in terms of volumetric water content (VWC), to allow for direct comparison with published data.

4.1 Water content–resistivity relationship

Figure 3 includes three laboratory-derived resistivity–water content curves: two- and four-point resistivity measurements made using the bespoke resistivity test chambers, and two-point measurements made on

cylindrical specimens with the addition of the conductive gel. It can be seen that there is close agreement between the two-point resistivity dataset and published data (McCarter [37]), showing an inverse power relationship with a sharp increase in resistivity at water contents below approximately 20%. The application of conductive gel to the disc electrodes has succeeded in improving contact with the soil, as is evident from the cylindrical specimen dataset having lower resistivity values than the other two-point dataset. Results gathered using the four-point method show lower values of resistivity to those from the two-point method and compare very well with measured in situ field data. The four-point values deviate from the two-point results considerably at water contents less than approximately 22%. However, approaching saturation, the two methods converge.

4.2 Effects of macro-cracks on resistivity

Figure 4 shows a drying curve comparing intact specimens and those with inbuilt horizontal fracture planes (orthogonal to the current flow). As can be seen in the figure, fractured specimens exhibited higher values of resistivity for a given water content, consistent with an increased porosity as air within the voids acts to impede current flow. Error bars of ±14% shown on the figure demonstrate that this shift in values is significant.

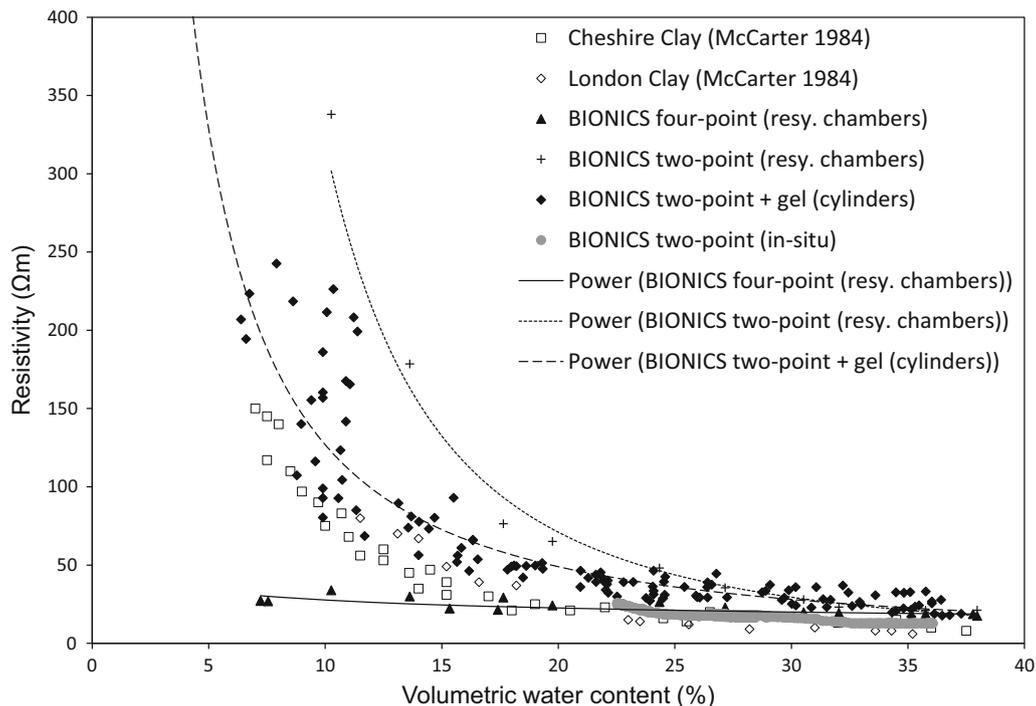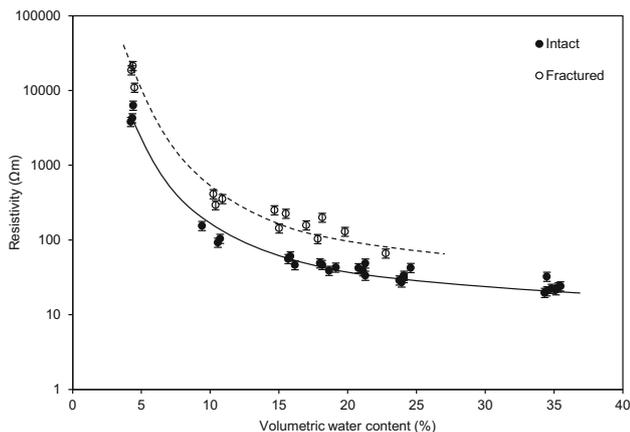**Fig. 3** Water content–resistivity relationship for BIONICS clay compared to published data

Fig. 4 Comparison of water content–resistivity relationship for fractured and intact specimens (two-point resistivity method)

4.3 Cyclic water content–resistivity relationship

In Fig. 5, the water content–resistivity data are shown. Little difference can be seen between drying and wetting paths, in keeping with Muñoz-Castelblanco et al. [40]; however, if the data are divided broadly into Stages 1 and 2 (each comprising a full dry-wet cycle, see Table 1), then a hysteretic inverse power relationship is evident. There is a shift of the resistivity–water content path centred at approximately 22% VWC, such that below this point, Stage 2 specimens have elevated values of resistivity with respect to Stage 1, with the opposite being true beyond this point, as is illustrated by two grey arrows. As before, resistivity error bars of ±14% show that this shift is likely to be significant.

4.4 Water content–shear strength relationship

In Fig. 6, a hysteretic relationship is shown between water content and shear strength, for repeated dry-wet cycles. For all four dry-wet cycles, shear strength is shown to decrease linearly with increasing water content. Both stages exhibit a drop in shear strength at the transition from a drying to wetting cycle, illustrated by a grey arrow. Stage 2 shear strength values are reduced with respect to Stage 1, but exhibit scanning-type behaviour: at approximately 22% water content, 2a converges with 1a and 2b converges with 1b, such that beyond this water content, there exists only one drying path and one wetting path, which converge approaching saturation. The reasons for this behaviour are discussed in Sect. 5.2.

4.5 Shear strength–resistivity relationship

Figure 7 shows a hysteretic shear strength–resistivity relationship, for ongoing seasonal cycling. As specimens are dried, there is an associated increase in both soil resistivity and shear strength. At the transition from a drying to a wetting cycle, there is a drop in C_u, illustrated by a grey arrow, after which specimens following a wetting path exhibit higher values of resistivity for a given shear strength than those following a drying path. As in Fig. 6, the Stage 2 re-drying and re-wetting paths demonstrate scanning-type behaviour and converge with their Stage 1 counterparts at shear strengths of 700 and 500 kPa, respectively. These behaviours are discussed in Sect. 5.3.
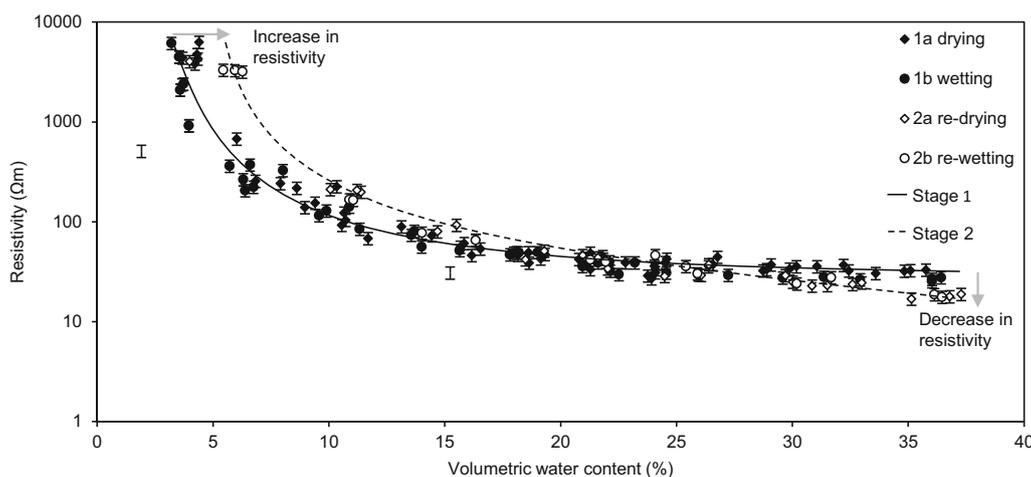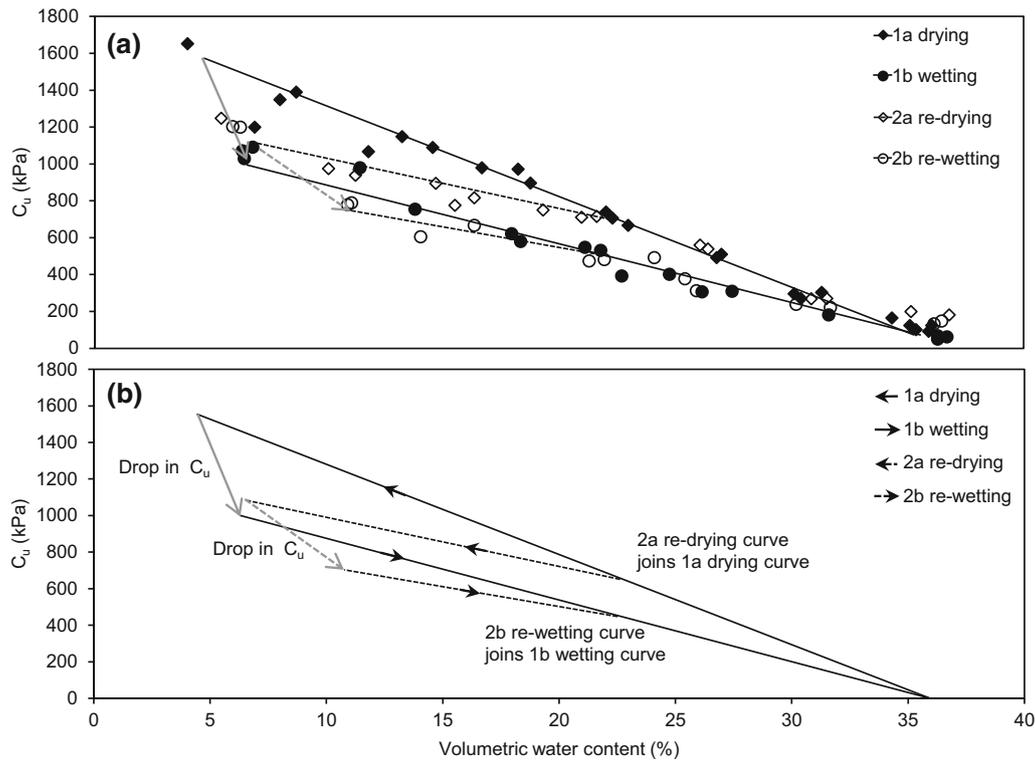

Fig. 5 Water content–resistivity relationship separated by seasonal stage (two-point resistivity method). Two trend lines have been fitted, highlighting Stages 1 and 2

Fig. 6 Water content–shear strength relationship for four seasonal cycles. **a** Data points with fitted linear trend lines. **b** Data points removed to highlight trend

4.6 Soil water retention curve

The WP4 dewpoint potentiometer was used to measure suction values, which were subsequently fitted using the van Genuchten [53] expression. Both continuous drying and wetting paths were fitted using the van Genuchten fitting parameters $n = 1.54$, $\alpha = 0.0097$ m^{-1} and $n = 1.29$, $\alpha = 0.1001$ m^{-1}, respectively (where $m = 1 - 1/n$), as can be seen in Fig. 8. The drying curve rapidly de-saturates from $\theta_s = 0.36$ at an approximate air entry value of 600 kPa. The drying path is shown to fit well, though the wetting path suffers from a reduced number of data points. However, in the measured suction range, the fitted curve is shown to pass through the majority of points. Traditionally, for the wetting path, re-saturated water content is observed to be reduced from the initial content due to the entrapment of air. The presented curve displays an inferred, elevated re-saturated water content on the wetting path considered as a product of increased porosity as a direct result of the formation of micro-cracking and permanent fabric modification, as described in Sect. 4.5. This trend is predicted due to the extreme drying (desiccation) that the specimens had undergone during the latter stages of drying prior to re-wetting. However, limitations in the dewpoint potentiometer

technique do not allow behaviour at very low suctions to be accurately investigated.

4.7 Soil fabric imaging

Figure 9a displays an E-SEM image of a specimen that has undergone drying in the E-SEM chamber. A clearly visible crack produced as a result of desiccation can be seen that is approximately 800 μm long and 50 μm wide. Upon closer inspection of this feature (Fig. 9b), particles lining the crack wall are shown to have aligned during drying-induced shrinkage and have created a distinct "coating" to the crack surface. After the specimen was removed from the E-SEM and rehydrated by the application of a distilled water droplet and left to homogenise overnight, the specimen surface was again scanned. Figure 9c shows a sample that exhibits a much more hydrated clay texture that is centred about a relic crack feature. This location is further magnified in Fig. 9d and demonstrates both the partial closure and apparent infilling of the previously wider crack aperture. However, such a feature has remained identifiable and is likely to be a product of the permanent realignment of particles at the crack wall. It is therefore anticipated that this discontinuity would be exploited upon re-drying.
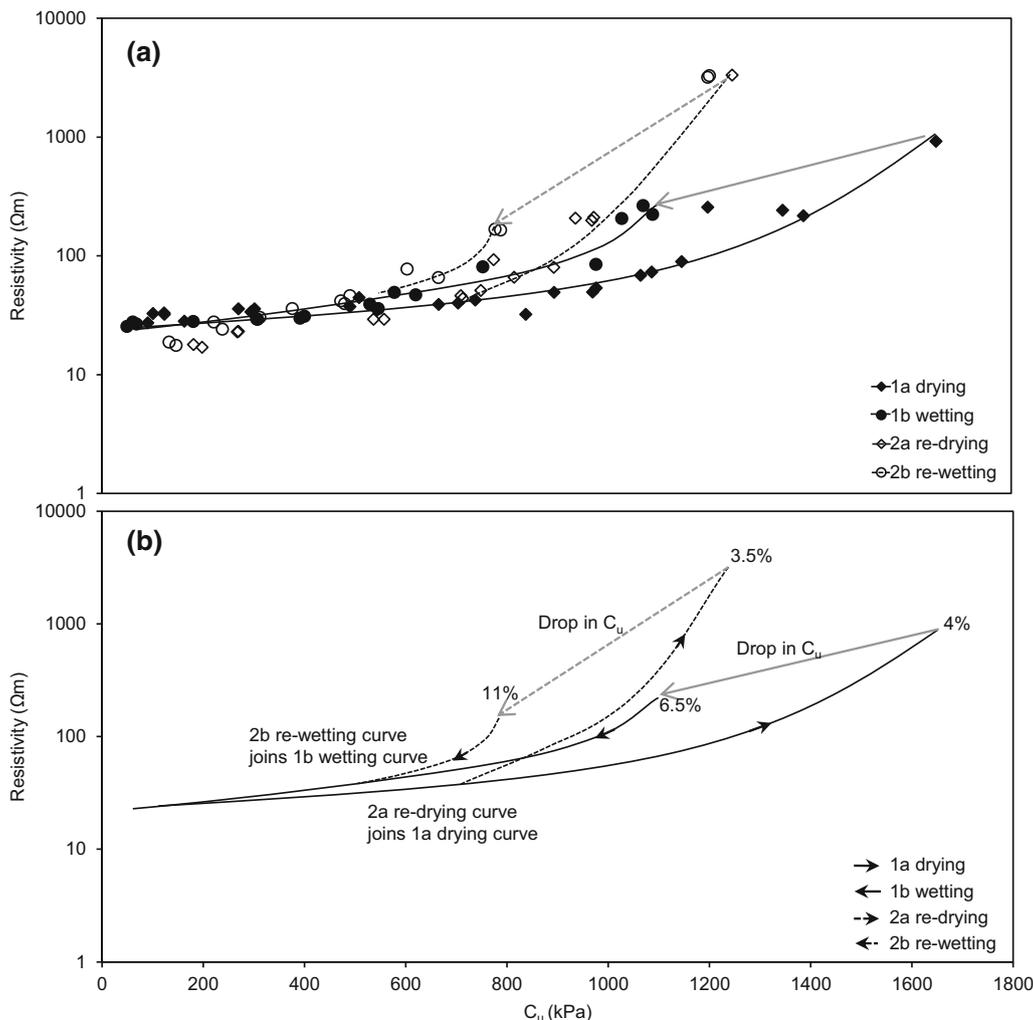
Fig. 7 Resistivity–shear strength relationship (two-point resistivity method) for four seasonal cycles. **a** Data points with fitted trend lines. **b** Data points removed to highlight trend. Volumetric water contents are indicated across the transition boundaries in **b**

5 Discussion

5.1 Comparison of resistivity methods

Both of the previous studies presented in Fig. 3 (from McCarter [37]) made two-point resistivity measurements using plate electrodes, similar to the disc electrode method used in this study. This method relies on a relatively large area of contact between the plate electrodes and the soil specimen. At low water contents, contact resistances may be considerable, due to reduced coupling between the specimen and the electrode, and to a decreased contact area resulting from shrinkage. This results in high apparent resistivity measurements not representative of the soil mass as a whole and explains the sharp increase in resistivity values with decreasing water content observed from both the two-point datasets. The use of a four-point measure of transfer resistance, however, eliminates the contact

resistance effect [29], yielding far lower soil resistivity values, as can be seen from Fig. 3. Due to the fact that both two- and four-point tests were performed on the same specimens (using the resistivity test chambers), the authors conclude that the observed difference between the methods is indeed a direct result of the inclusion of contact resistances using the former method. Nearing saturation, the difference between the two methods is less pronounced as the presence of water acts as a coupling agent at the specimen-electrode interface. Field measurements obtained from the Decagon 5TE sensors (which also make two-point measurements) exhibit values of resistivity closer to those of the four-point dataset, which was attributed in part to low in situ anisotropy and very low contact resistances due to good soil–sensor contact resulting from the sensors being embedded at depth.

From Fig. 3, it is plain that the two-point method overestimates resistivity values at lower water contents,
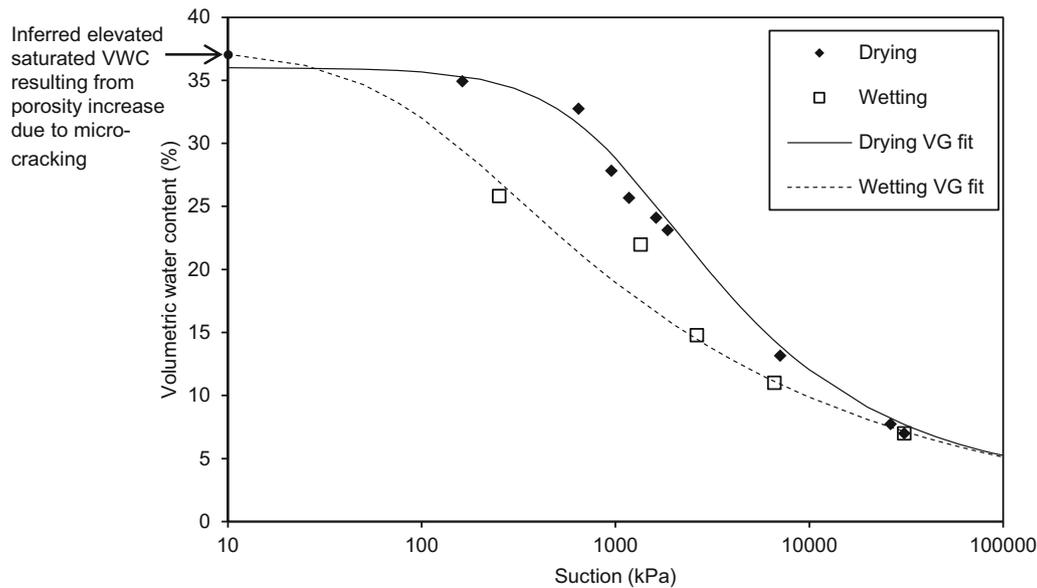
Fig. 8 Soil water retention curve

and therefore constitutes a bulk measurement not representative of true soil resistivity at low moistures. Despite this overestimation, however, the method can still be used to provide qualitative information, regarding trends in the evolution of soil resistivity. This inverse power relationship between resistivity and water content apparent from both methods is suggested to be a function of the combination of several effects:

1. An increase in contact resistance resulting from reduced coupling at the soil–electrode interface at low water contents;
2. Reduced bulk mobility at low water contents of ions present in the soil dissolved in the pore water;
3. The development of fractures in the soil which impede current flow, due to the volume-sensitive nature of the test material.

5.2 Effect of dry-wet cycling on geophysical–geotechnical relationships

Due to its volume sensitivity, desiccation cracking is associated with clay subjected to dry-wet cycles, as discussed in Sect. 1. In Fig. 4, the water content–resistivity relationship for deliberately fractured specimens is presented alongside that for intact specimens, showing elevated values of resistivity resulting from macro-cracking due to the insulating nature of air, impeding current flow. This observation implies that the presence of tension or desiccation cracks in the near surface could be identified from high resistivity anomalies captured by ERT imaging of clay slopes.

In addition to this macro-scale cracking, it is pertinent to consider desiccation cracking at the micro-scale: in keeping with Muñoz-Castelblanco et al. [40], no hysteresis could be observed from Fig. 5 when considering separate drying and wetting paths, inferring that resistivity is independent of soil suction. However, if the water content–resistivity relationship of the test material is separated broadly into two main stages (each comprising a full dry-wet cycle), a hysteretic shift of the path is observed: below approximately 22% VWC, specimens subjected to more than one dry-wet cycle have increased values of resistivity with respect to those subjected to less than one. This increase is suggested to be attributable to the development of fissures at the scale of the soil fabric itself.

Interestingly, at water contents beyond 22% VWC, specimens subjected to more than one dry-wet cycle exhibit resistivity values lower than those subjected to fewer than one. A suggestion for this reversal between the two phases at high water contents is the dissolution of clay particles in the pore water, such that they become further mobilised with ongoing dry-wet cycling, with existing cracks acting as a high conductivity conduit upon filling with water.

The hysteresis observed from Fig. 5 is supported by Fig. 9, which illustrates the evolution of soil fabric changes during a seasonal cycle: Fig. 9b shows a desiccation fissure with a distinct coating of clay particles along its walls, whilst the fissure shown in Fig. 9d (after the addition of water) shows no coating (suggesting that it has been dissolved) and appears in be partially infilled, which may act as a conduit for additional current flow. Effectively, a clay film is developed during drying, which is mobilised into the pore water during imbibition, increasing its conductivity.
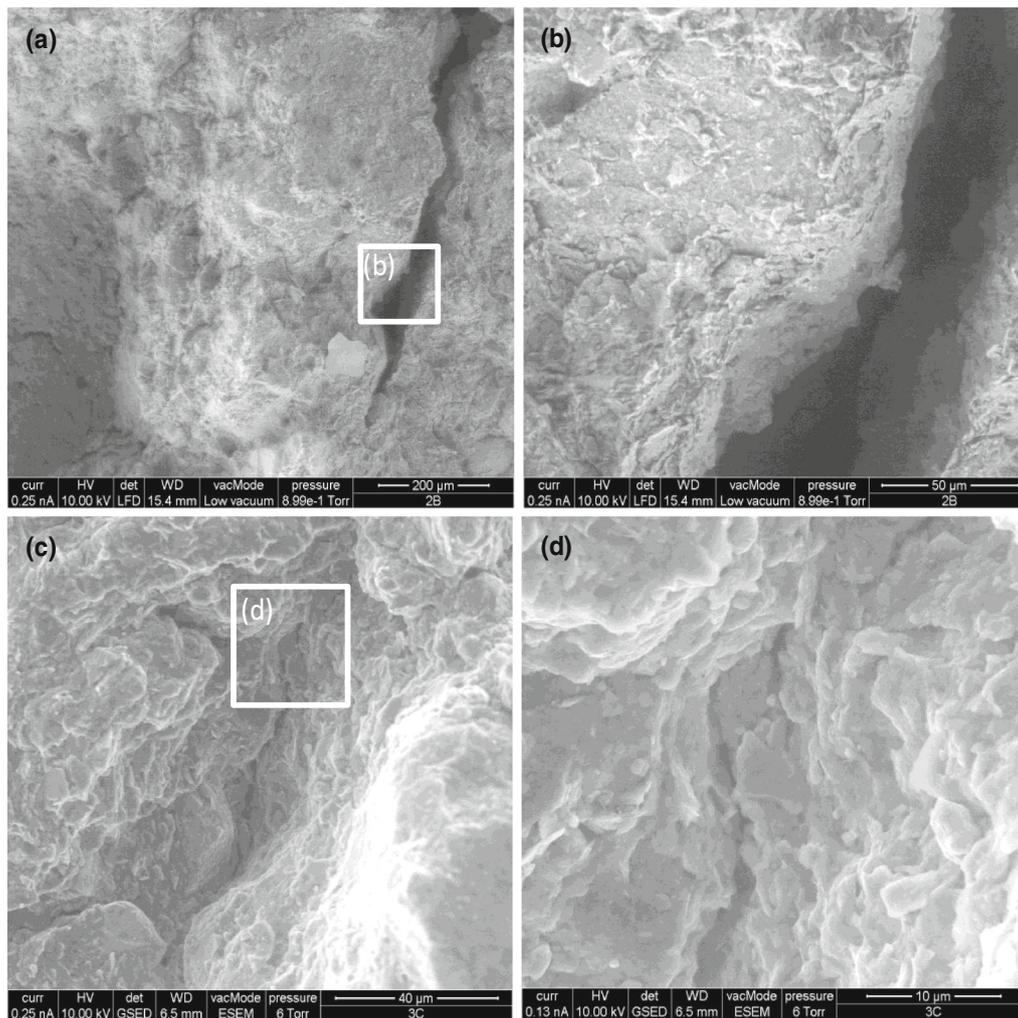
Fig. 9 E-SEM images taken at two sites, illustrating **a** Site 1 after 90 min at 10% RH, and showing the position of **b** desiccated clay particles and fracture wall under higher magnification. **c** Site 2, showing of reduced crack aperture following re-wetting and the position of **d** hydrated particles under higher magnification

Further evidence for desiccation cracking at the micro-scale is provided by the shear strength response to dry-wet moisture cycles, given in Fig. 6, showing hysteresis of the linear shear strength–water content relationship for successive cycles. It can be observed that the primary and secondary drying curves (Stages 1a and 2a, respectively) follow the same initial path, but then deviate at water contents less than approximately 22% VWC, when the Stage 2a gradient decreases. The same is observed between primary and secondary wetting stages (Stages 1b and 2b, respectively). 22% VWC has already been identified as the transition between continuity and discontinuity of the water phase within the soil, but due to the decrease in the shear strength gradient, it can also be considered as the point at which fractures develop (and heal) in the soil, as the water meniscus is broken: cracks form along the initial drying path, heal along the subsequent wetting path, and reopen

along the secondary drying path (at 22%), with new cracks also forming. This soil fabric deterioration is supported by Fig. 9, which indicates a fundamental change in the micro-scale structure of high clay content material, when subjected to dry-wet cycles. By imaging the grain-scale structure of this material subjected to drying, the formation of permanent discontinuities is confirmed.

In addition to soil fabric deterioration promoting a reduction in shear strength, the role of soil water retention must be considered. Hysteresis of the soil water retention curve between drying and wetting is well understood [20, 22, 49] and is apparent in Fig. 8, as suctions developed in the soil during drying cannot be recovered during wetting, due to entrapped air. Figure 6b illustrates the sudden drop in shear strength at the transition boundary from a drying to a wetting cycle, whereafter specimens resume a linear wetting path. Near this boundary, specimens of equivalent water

content on both drying and wetting paths will have similar fracture densities; therefore, soil fabric deterioration does not explain the shear strength loss. The concept of reduced suctions along the wetting path is supported by the Stage 2a (re-drying) path exhibiting elevated shear strengths with respect to the Stage 1b (wetting) path: specimens are wetted up to saturation, effectively "resetting" their saturation history and then dried out again, yielding strengths above those of the preceding wetting path.

In summary, two potential mechanisms exist for the reduction in soil strength apparent in Fig. 6: suction loss due to hysteretic soil–water retention behaviour, and soil fabric deterioration via the development of micro-scale cracks, as discussed above.

5.3 Implications for ERT

The main reason for investigating how the various parameters considered in this study interact with each other is to fully analyse electrical resistivity data gathered from electrical resistivity tomography, with respect to slope stability assessment. Ultimately, the goal of ERT in this context is to make inferences about the strength of the subsurface itself.

The mechanisms by which water directly affects soil resistivity and strength are well understood (as discussed in Sect. 1), but no direct relationship exists between shear strength and resistivity. However, even though these two parameters do not impact on each other directly, it is possible to resolve a relationship between them as is presented in Fig. 7, for two full cycles of drying and wetting. From this relationship, both the following may be observed: the drop in shear strength at the transition from drying to wetting events attributed to hysteretic soil water retention behaviour; and elevated resistivity values with corresponding decreased shear strengths resulting from soil fabric deterioration. At the transition from Stage 1a (drying) to Stage 1b (wetting), there is a considerable loss in shear strength from approximately 1650 to 1100 kPa, and although there is also a fall in the corresponding resistivity values, this is attributed to the increase from 4 to 6.5% VWC, rather than being a function of suction loss. Soil resistivity was established to be independent of soil suction in Sect. 5.2, thus fluctuations in pore pressure will only be reflected in resistivity values if there is also a significant variation in water content, but as shown above, even a relatively small moisture increase can drastically reduce soil strength. Therefore, an ERT system installed in the field will not be capable of capturing potentially considerable changes in soil pore pressure at the onset of a wetting event (i.e. heavy rain) which may precede a slope failure event, unless the soil's saturation history is accounted for.

The in situ relationship between resistivity and water content may change over time due to the cumulative effect of soil fabric changes induced by seasonal cycles of drying and wetting, particularly in the near surface. If ERT data are to be used to estimate soil water content, then this "ageing" effect (as in Delage et al. [16]) may be significant over long time periods. Although the soil water retention curve may also change over time, in most cases, fill material will have undergone a large number of dry-wet cycles; therefore, a residual SWRC may be appropriate, comprising both a drying and wetting path; in more recently constructed slopes, or in natural slopes exposed to a changing climate, a changing SWRC may be required. If ERT-derived water content values are to be resolved into pore water pressures using soil water retention curves, then antecedent groundwater conditions must also be measured so that the appropriate drying or wetting curve is used. The implication of the above is that if ERT is to be used to predict imminent slope failure, then it is essential that systems should be installed in parallel with basic weather monitoring equipment (rain gauges) and/or geotechnical point sensors so that the appropriate wetting or drying curves are used.

This study has been successful in employing a comprehensive, multi-scalar approach to resolve the geophysical–geotechnical relationships essential to using ERT for assessment of slope stability; however, further work is required. It has been shown that soil fabric deterioration has a cumulative effect to reduce shear strength over time, with the simultaneous evolution of resistivity. Therefore, a more detailed knowledge of near-surface soil deterioration is also required if ERT is to be used over long time periods. Indeed, ERT itself could prove useful in the assessment of this deterioration in situ. Although the material used in this study was deemed to be representative of UK glacial tills used in earthwork construction, if ERT is to be used in large-scale slope assessments across the UK then it will be necessary to establish the relevant geophysical–geotechnical relationships for a range of representative engineering soils.

6 Conclusions

In this study, a rigorous testing programme has been undertaken, integrating the results of multi-scalar laboratory and field experiments, at a range of saturation states. A series of preliminary proxies for analysing ERT data in the context of slope stability has been established, incorporating the effects of both soil water retention behaviour and deterioration of soil fabric over time. From this study, the following conclusions have been drawn:

1. A comparison of resistivity methods showed significantly elevated values when making a two-point rather than a four-point measurement, resulting from contact resistance effects at low water contents associated with the former. Current standard practice describes a two-point measurement, but given that the four-point method circumvents the effects of contact resistance, a review of the advocated standard practice (as described in BS1377-3) to indicate potential limitations and resistivity overestimation at low water contents is suggested.

2. An inverse power relationship was observed between soil resistivity and water content, shown to be independent of soil suction. The relationship was, however, observed to be hysteretic for repeated dry-wet cycles, suggested to be evidence of soil fabric deterioration as micro-cracks develop in the clay and act to impede current flow, increasing soil resistivity at low water contents. At high water contents, soil resistivity was observed to decrease with ongoing seasonal cycling, suggested to be due to the dissolution of clay particles into the pore water, which then fill existing micro-cracks, providing a conduit for additional current flow. These trends were supported by micro-scale images obtained from scanning electron microscopy. Shear strength was shown to be principally affected by two mechanisms: hysteretic soil water retention behaviour resulting in suction loss at the transition from drying to wetting events, and soil fabric deterioration with ongoing seasonal cycling.

3. If ERT systems are to be used in the assessment of slope stability, both saturation history and soil fabric deterioration must be considered. Therefore, ERT systems must be used in conjunction with basic geotechnical monitoring equipment (e.g. rain gauges, point sensors) to identify either drying or wetting behaviour. The long-term effects of this deterioration require further investigation, which could be achieved in situ using ERT systems.

4. This study has been successful in resolving the preliminary geophysical–geotechnical relationships essential to the development of an ERT-based slope stability assessment system. Amidst future climate change projections which imply potentially widespread slope failure, risk-based early interventions are of paramount importance to prevent failure of these geotechnical assets, with repairs costing up to ten times as much as preventative action. Geoelectrical imaging using electrical resistivity tomography may be used to identify the changes in internal ground conditions that precede failure, allowing risk to be assessed, which current systems are unable to accomplish. This research constitutes a study of one type of soil; however, for such a system to be viable across the UK, it will be necessary to establish the relevant geophysical–geotechnical relationships for range of representative engineering soils.

References

1. American Society for Testing and Materials (1985) ASTM D2487–11: Standard practice for classification of soils for engineering purposes (Unified Soil Classification System). ASTM International, West Conshohocken

2. Archie GE (1942) The electrical resistivity log as an aid in determining some reservoir characteristics. Trans AIME 146:54–62

3. Binley A, Hubbard SS, Huisman JA, Revil A, Robinson DA, Singha K, Slater LD (2015) The emergence of hydrogeophysics for improved understanding of subsurface processes over multiple scales. Water Resour Res. doi:10.1002/2015WR017016

4. Birch G, Anderson I (2011) LiDAR monitoring for the Folkestone Warren landslide. Ground Engineering, May 2011. https://www.newcivilengineer.com/download?ac=1378994. Accessed 1 June 2015

5. British Standards Institution (1990) BS 1377-2: methods of test for soils for civil engineering purposes part 2: classification tests. BSI, Milton Keynes

6. British Standards Institution (1990) BS 1377-3: methods of test for soils for civil engineering purposes part 3: chemical and electro-chemical tests. BSI, Milton Keynes

7. British Standards Institution (1990) BS 1377-4: methods of test for soils for civil engineering purposes part 4: compaction-related tests. BSI, Milton Keynes

8. British Standards Institution (1990) BS 1377-7: methods of tests for soils for civil engineering purposes part 7: shear strength tests (total stress). BSI, Milton Keynes

9. Chambers JE, Gunn DA, Wilkinson PB, Meldrum PI, Haslam E, Holyoake S, Kirkham M, Kuras O, Merritt A, Wragg J (2014) 4D electrical resistivity tomography monitoring of soil moisture dynamics in an operational railway embankment. Near Surf Geophys 12:61–72

10. Chambers JE, Wilkinson PB, Kuras O, Ford JR, Gunn DA, Meldrum PI, Pennington CVL, Weller AL, Hobbs PRN, Ogilvy RD (2011) Three-dimensional geophysical anatomy of an active landslide in Lias Group mudrocks, Cleveland Basin, UK. Geomorphology 125:472–484

11. Chrétien M, Lataste JF, Fabre R, Denis A (2014) Electrical resistivity tomography to understand clay behavior during seasonal water content variations. Eng Geol 169:112–123

12. Cui YJ, Tang AM, Mantho A, De Laure E (2008) Monitoring field soil suction using miniature tensiometer. Geotech Test J 31(1):95–100

13. Decagon Devices (2014) WP4C Dewpoint potentiometer, operator's manual. Decagon Devices Inc. http://manuals.decagon.com/Manuals/13588_WP4C_Web.pdf. Accessed 1 June 2015

14. Decagon Devices (2015) 5TE Soil moisture, temperature and electrical conductivity sensor, operator's manual. Decagon Devices Inc. http://manuals.decagon.com/Manuals/13509_5TE_Web.pdf. Accessed 1 June 2015

15. DEFRA (2009) Adapting to climate change: UK climate projections. DEFRA, London

16. Delage P, Marcial D, Cui YJ, Ruiz X (2006) Ageing effects in a compacted bentonite: a microstructure approach. Géotechnique 56(5):291–304

17. Dijkstra T, Dixon N, Crosby C, Frost M, Gunn D, Fleming P, Wilks J (2014) Forecasting infrastructure resilience to climate change. P I Civ Eng-Trans 167(5):269–280. ISSN: 0965-092X. doi: 10.1680/tran.13.00089

18. Driscoll R (1983) The influence of vegetation on the swelling and shrinking of clay soils in Britain. Géotechnique 33:93–105

19. Dunnicliff J (1988) Geotechnical instrumentation for measuring field performance. Wiley, New York

20. Fredlund DG, Sheng D, Zhao J (2011) Estimation of soil suction from the soil water characteristic curve. Can Geotech J 48:186–198

21. Fredlund DG, Rahardjo H (1993) Soil mechanics for unsaturated soils. Wiley, New York

22. Fredlund DG, Xing A (1994) Equations for the soil-water characteristic curve. Can Geotech J 31(4):521–532

23. Friedel S, Thielen A, Springman SM (2006) Investigation of a slope endangered by rain-fall-induced landslides using 3D resistivity tomography and geotechnical. J Appl Geophys 60(2):100–114

24. Fukue M, Minatoa T, Horibe H, Taya N (1999) The microstructure of clay given by resistivity measurements. Eng Geol 54:43–53

25. Gunn DA, Chambers JE, Uhlemann S, Wilkinson PB, Meldrum PI, Dijkstra TA, Haslam E, Kirkham M, Wragg J, Holyoake S, Hughes PN, Hen-Jones R, Glendinning S (2014) Moisture monitoring in clay embankments using electrical resistivity tomography. Constr Build Mater 92:82–94

26. Glendinning S, Hall J, Manning L (2009) Asset-management strategies for infrastructure embankments. P I Civ Eng Eng Sustain 162(2):111–120

27. Glendinning S, Hughes PN, Helm P, Chambers J, Mendes J, Gunn D, Wilkinson P, Uhlemann S (2014) Construction, management and maintenance of embankments used for road and rail infrastructure: implications of weather induced pore water pressures. Acta Geotech 9(5):799

28. Hassan A (2014) Electrical resistivity method for water content characterisation of unsaturated clay soil. PhD Thesis, Durham University. http://etheses.dur.ac.uk/10806/. Accessed 9 Aug 2015

29. Heaney BM (2003) Electrical Conductivity and resistivity. In: Webster JG (ed) Electrical measurement, signal processing, and displays. CRC Press, Boca Raton, pp 1–14

30. Hughes PN, Glendinning S, Mendes J, Parkin G, Toll DG, Gallipoli D, Miller P (2009) Full-scale testing to assess climate effects on embankments. P I Civ Eng Eng Sustain 162(2):67–79

31. Jaboyedoff M, Demers D, Locat J, Locat A, Locat P, Oppikofer T, Robitaille D, Turme D (2009) Use of ground-based LIDAR for the analysis of retrogressive landslides in sensitive clay and of rotational landslides in river banks. Can Geotech J 46(12):1379–1390

32. Kavian M, Slob EC, Mulder WA (2011) Hysteresis in the non-monotonic electric response of homogeneous and layered unconsolidated sands under continuous flow conditions with water of various salinities, 100 kHz to 2MHz. J Geophys Res 116:B08214

33. Kibria G, Hossain M (2012) Investigation of geotechnical parameters affecting electrical resistivity of compacted clays. J Geotech Geoenviron 138(12):1520–1529

34. Knight R (1991) Hysteresis in the electrical resistivity of partially saturated sandstones. Geophysics 56:2139–2147

35. Loke MH, Chambers JE, Rucker DF, Kuras O, Wilkinson PB (2013) Recent developments in the direct-current geoelectrical imaging method. J Appl Geophys 95:135–156

36. Loveridge FA, Spink TW, O'Brien AS, Briggs KM, Butcher D (2010) The impact of climate and climate change on infrastructure slopes, with particular reference to Southern England. Q J Eng Geol Hydroge 43(4):461–472

37. McCarter WJ (1984) Electrical resistivity compacted clays. Géotechnique 34(2):263–267

38. Merritt AJ, Chambers JE, Murphy W, Wilkinson PB, West LJ, Gunn DA, Meldrum PI, Kirkham M, Dixon N (2014) 3D ground model development for an active landslide in Lias mudrocks using geophysical, remote sensing and geotechnical methods. Landslides 11:537–550

39. Michot D, Benderitter Y, Dorigny A, Nicoullaud B, King D, Tabbagh A (2003) Spatial and temporal monitoring of soil water content with an irrigated corn crop cover using electrical resistivity tomography. Water Resour Res 39(5):1138

40. Muñoz-Castelblanco J, Pereira J, Delage P, Cui YJ (2012) The influence of changes in water content on the electrical resistivity of a natural unsaturated loess. ASTM Geotech Test J 35(1):11–17

41. Newgate Online (2016) Nyogel 756G, 100 gram tube. Available at http://newgateonline.com/nyogel-756g-100gram-tube.html. Accessed 20 Apr 2016

42. Perrone A, Lapenna V, Piscitelli S (2014) Electrical resistivity tomography technique for landslide investigation: a review. Earth-Sci Rev 135:65–82

43. Perry J, Pedley M, Reid M (2001) Infrastructure embankments: condition appraisal and remedial treatment. CIRIA, London, Report C550

44. Rail Accident and Investigations Branch (RAIB) (2008) Network Rail's management of existing earthworks. Department for Transport, London

45. Roberts JJ, Lin W (1997) Electrical properties of partially saturated Topopah Spring Tuff: water distribution as a function of saturation. Water Resour Res 33(4):577–587. doi:10.1029/96WR03905

46. Russell EJF, Barker RD (2010) Electrical properties of clay in relation to moisture loss. Near Surf Geophys 8:173–180

47. Samouelian A, Cousin I, Tabbagh A, Bruand A, Richard G (2005) Electrical resistivity survey in soil science: a review. Soil Tillage Res 83:173–193

48. Shevnin V, Mousatov A, Ryjov A, Delgado-Rodriquez O (2007) Estimation of clay content in soil based on resistivity modelling and laboratory measurements. Geophys Prospect 55:265–275

49. Šimůnek J, Kodešová R, Gribb M, Van Genuchten MT (1999) Estimating hysteresis in the soil water retention function from cone permeameter experiments. Water Resour Res 35(5):1329–1345

50. Stirling RA, Davie CT, Glendinning S (2013) Numerical modelling of desiccation crack induced permeability. In: Proceedings

of the 18th international conference on soil mechanics and geotechnical engineering, Paris 2013, pp 813-816

51. Stirling RA, Hen-Jones RM (2015) Investigating geotechnical/geophysical relationships in unsaturated glacial till–COST Action TU1202: Short Term Scientific Mission Report. doi: 10.13140/RG.2.1.2703.3769

52. Toll DG, Lourenço SDN, Mendes J, Gallipoli D, Evans FD, Augarde CE, Cui YJ, Tang AM, Rojas JC, Pagano L, Mancuso C, Zingariello C, Tarantino A (2011) Soil suction monitoring for landslides and slopes. Q J Eng Geol Hydrogeol 44(1):23–33

53. Van Genuchten MT (1980) A closed-form equation for predicting the hydraulic conductivity of unsaturated soils. Soil Sci Soc Am J 44(5):892–898

54. Waxman MH, Smits LJM (1968) Electrical conductivities in oil-bearing shaly sands. Soc Petrol Eng J 8:107–122

55. Wood DM (1990) Soil behaviour and critical state soil mechanics. University Press, Cambridge

56. Yamakawa Y, Kosugi K, Masaoka N, Sumida J, Tani M, Mizuyama T (2012) Combined geophysical methods for detecting soil thickness distribution on a weathered granitic hillslope. Geomorphology 145–146:56–69